Journal of the Korean Vacuum Society
Vol. 3, No. 2, June 1994, pp. 212-219

〈연구논문〉

Structure and Photoluminescence of ZnS-ZnSe Superlattices Grown by Hot Wall Epitaxy

Y. D. Choi, S. Sakakibara*, K. Ishino*, A. Ishida* and H. Fujiyasu*

Department of Physics, Mokwon University, Taejon 301-729, Korea
**Department of Electronics, Faculty of Engineering, Hamamatsu 432, Japan*
(Received April 25, 1994)

Hot Wall Epitaxy에 의하여 성장된 ZnS-ZnSe 초격자의 구조 및 Photoluminescence

최용대 · S. Sakakibara* · K. Ishino* · A. Ishida* · H. Fujiyasu*

목원대학교 물리학과
**Department of Electronics, Faculty of Engineering, Hamamatsu 432, Japan*
(1994년 4월 25일 접수)

Abstract — ZnS-ZnSe superlattices(SLs) were grown on the GaAs(100) by hot wall epitaxy. The period of ZnS-ZnSe SLs grown was confirmed by X-ray diffraction patterns, and compared with the theoretical pattern calculated considering the strain. It was calculated that the strain ratios of ZnS and ZnSe parallel to interfaces are decreased with increasing the ZnS thickness for ZnSe one. The photoluminescence(PL) of ZnS-ZnSe SLs consists of a sharp line in the high energy region and of broad spectra in the lower energy region. The peak photon energy of ZnS-ZnSe PL was compared with the energy of the theoretical calculations using Kronig-Penney model, and ZnS-ZnSe SLs were considered to be type I.

요 약 — Hot wall epitaxy법에 의하여 GaAs(100)면 위에 ZnS-ZnSe 초격자를 성장하였다. ZnS-ZnSe 초격자의 주기는 x-선 회절 패턴에 의하여 확인되었고, 이것은 변형을 고려하여 계산된 이론적인 패턴과 비교되었다. 경계면에 평행한 ZnS와 ZnSe의 변형의 비는 ZnSe에 대하여 ZnS의 두께가 증가할수록 감소되었다. ZnS-ZnSe 초격자의 photoluminescence(PL)는 고에너지 영역의 예리한 스펙트럼과 저에너지 영역의 폭이 넓은 스펙트럼으로 구성되어 있다. PL의 광자 에너지는 Kronig-Penney 모델을 사용하여 계산된 이론적인 에너지 값과 비교한 결과 type I의 초격자임을 알았다.

1. Introduction

ZnS-ZnSe quantum wells (QWs) and superlattices (SLs) of II-VI compounds have recently been widely studied by many research groups using different methods such as hot wall epitaxy (HWE) [1], molecular beam epitaxy (MBE) [2], and metal organic chemical-vapor deposition [MOCVD] [3].

ZnS-ZnSe SLs have been of great interest because they posses excellent luminescent properties for their applications to optoelectronic devices in the short wavelength region. However, it is difficult to control the electrical properties of ZnS-ZnSe because of the self-compensation and residual impurities [4]. To avoid these effects, HWE is preferable [1, 5].

Lattice mismatched heterostructures such as ZnS-ZnSe can be grown with essentially no misfit defect generation if the layers are sufficiently thin [6]. Although the lattice mismatch of ZnS-ZnSe SLs is somewhat large, 5%, strained-layer SLs are uniformly made. When SLs are formed, ZnSe layers

are compressed to enhance their bond energy and to reduce defect which are easily introduced into ionic crystals. While ZnS layers are subject to tensile strain. Structural analysis of the superlattice is very important in the research of physical properties and device application. X-ray analysis is one of the most important method to investigate the superlattice, especially for the analysis of the strained layer SLs [7].

The X-ray analysis gives very useful and exact information about the superlattice structure, strain, interdiffusion of the constituents, and also about fluctation of the superlattice period.

ZnS-ZnSe SLs applied to the devices are considered to show very weak photoluminescence (PL) associated with deep level defects. It was reported that strong PL associated with the band edges or with the excitons and weak PL associated with deep level defects were emitted by SLs of the thin ZnSe (<30 Å) and or of the thin ZnS(<30 Å). These facts indicate that strained SLs of the thin ZnSe and ZnS layers without introducing many defect are easily prepared [5].

In this study, the structure and PL of ZnS-ZnSe SLs grown by HWE are reported by the analysis of X-ray diffraction pattern and PL measurement. These results are compared with the theoretical calculation data taking into account the strain of the layers.

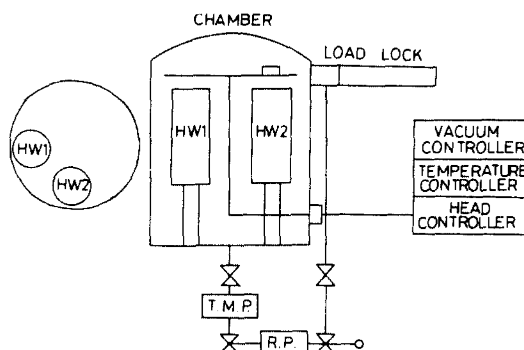

Fig. 1. Schematic diagram of HWE system to prepare ZnS-ZnSe SLs layer. Two HW furnaces are set on a concentric circle as shown in the left side.

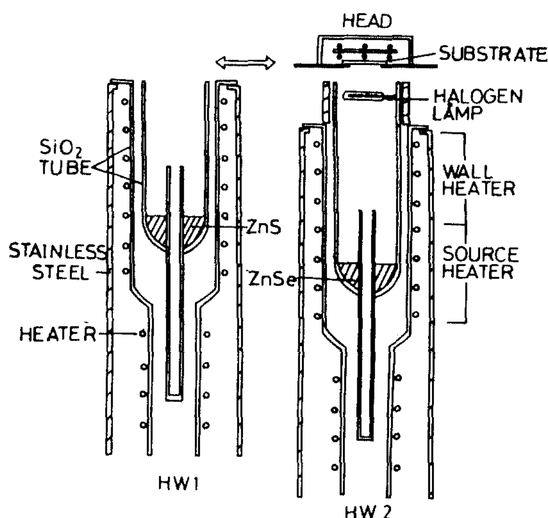

Fig. 2. Cross-section of the HW furnaces used to prepare ZnS-ZnSe SLs.

2. Sample Preparation

HWE is a convenient method to make not only high quality compound semiconductor films, but also SLs. [8] ZnS-ZnSe SLs were grown on Cr-doped semi-insulating GaAs(100) substrates using a model FHW 8700 (FUJI SEIKI Inc.) system. Fig. 1 shows a schematic diagram of HWE system to prepare ZnS-ZnSe SLs layer. The system consists of two independent hot wall (HW) furnaces for growing ZnS and ZnSe layer. Fig. 2 shows the cross section of the HW furnaces. For the preparation of ZnS-ZnSe SLs, the substrate was moved onto the outlet of each furnace.

For the growth of ZnS and ZnSe layer, the growth-interruption process was used. [9] This method means that the first buffer ZnS layer with the constants interval period on the GaAs(100) substrate, the next alternate ZnS and ZnSe layers are grown on the substrate sucessively. In this experimemt unlike the conventional method, the wall temperature of the furnace for the growing ZnSe layers was controlled by both the heater wire and halogen lamps. Halogen lamps greatly affected the growth rate and the morphology of ZnSe layers, and were installed to obtain photons to get high quality films. Polycrystalline ZnS and ZnSe as the source material of SLs were used. The substrates were cleaned by solvent, etched in $H_2SO_4 : H_2O : H_2O_2 =$

Table 1. ZnS-ZnSe SLs structures in the experiments

Sample	N_A (ZnS) Number of layer	N_B (ZnSe) Number of layer	Number of layer
#201	24	2	166
#204	19	2	166
#202	18	2	166
#203	18	3	160
#199	13	3	225

4 : 1 : 1, rinsed with deionizd H_2O. They were thermally cleaned at 550℃ for 10 minutes at a pressure of 2×10^6 Torr to remove the remaining oxide layer. During the growth the substrate temperature was kept at 250℃, while the wall and source temperature of ZnSe furnace were 660℃, respectively. Also, the wall and source temperature of ZnS source were 650℃, and 700℃, respectively. The thickness of the growing period layer was adjusted by controlling the growing time, using the basic growth rate data of ZnS and ZnSe monolayers. The growth rates of ZnS and ZnSe layer were almost 0.7 Å/sec and 2 Å/sec, respectively. SLs were grown on the ZnS buffer layer with the thickness of almost 3,500 Å to diminish the misfit of the lattice.

ZnS-ZnSe SLs structures were ascertained by observing X-ray diffraction satellities. PL spectra were measured at 77 K, and He-Cd laser as the light source was used. The samples used to measure are listed in Table 1.

3. Results and Discussion

3.1. X-ray diffraction pattern

First of all, the X-ray diffraction of the ZnS-ZnSe SLs is considered. Fig. 3 shows the superlattice structure and strain in the superlattice schematically. The number of atomic layers is represented as N_A and N_B, respectively, and lattice spacings perpendicular to the superlattice layer as $d_{\perp A}$ and $d_{\perp B}$, respectively. Cu($K\alpha_1$, $K\alpha_2$) radiation was used for the X-ray source. Fig. 4 shows X-ray diffraction patterns of ZnS-ZnSe SLs listed in Table 1. X-ray diffraction patterns of SLs with the (400) peaks of the substrate GaAs and the ZnS buffer layer are shown. There are some satellite peaks close to (400) peak of the buffer ZnS layer. These satellite peaks indicate to be a SLs structure. X-ray diffraction peaks appears near the angle θ where the equation $2D\sin\theta = n\lambda$ (n: integer, D: SLs period) is satisfied. The deviation of the peak from the calculated angle is generally small, but it becomes relatively large for the SLs with broad diffraction peaks. Lattice mismatch between the SLs and the substrate should affect the strain in the SLs layer. Different strains of different layers, near and away from the substrate, must broaden the width of the satellite spectrum [10]. The thicknesses (L_A+L_B) of layers (N_A+N_B) in Table 1 were obtained from the angle of these satellite peaks. The satellite peaks were shifted by the variation of the number of ZnS and ZnSe

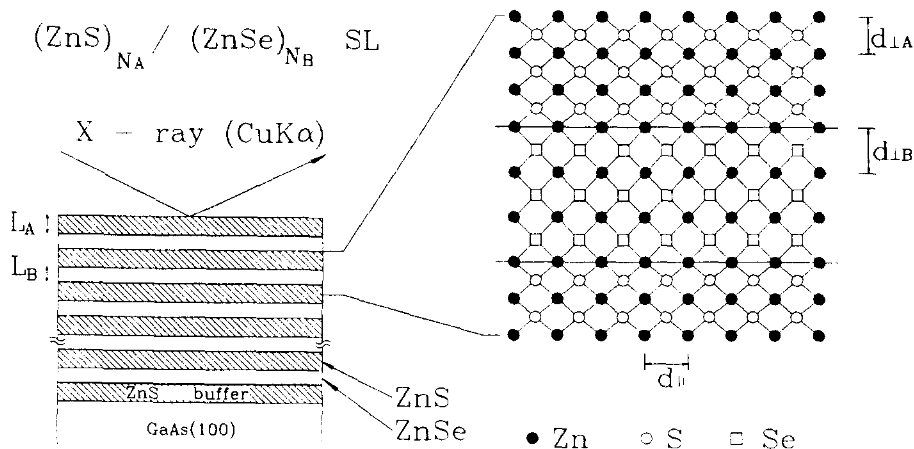

Fig. 3. Schematic superlattice structure and the strain in the superlattice.

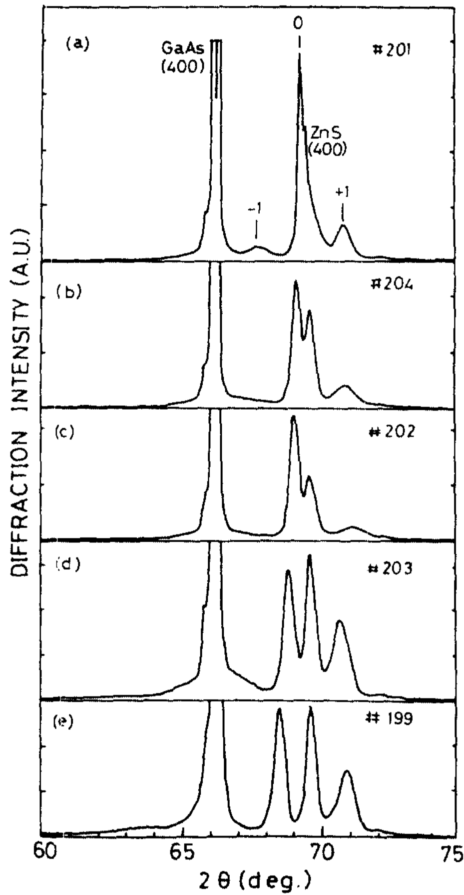

Fig. 4. X-ray diffraction pattern of ZnS-ZnSe SLs.

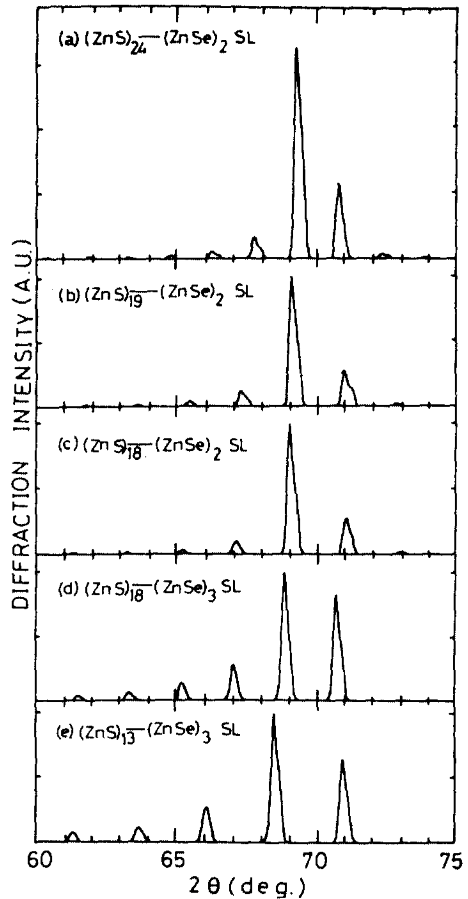

Fig. 5. X-ray diffraction pattern calculated by considering the strain.

layer, N_A, N_B. The strongest one of them was shifted towards low (high) angle as ZnSe(ZnS) layer was increased. Fig. 4(a) and (e) show that the period of the peaks of SLs increases(decreases) with decreasing(increasing) total thickness of ZnS and ZnSe layer. Fig. 4(b) and (d) indicate that although the periods of SLs are nearly equal, the peak positions and intensity are different. Fig. 5 shows the calculated diffraction patterns using the strain equation to determine the number of monolayer N_A, N_B in Fig. 4. The lattice constant $d_{\perp i}$ ($i=A$ or B) of the SLs is calculated from the parallel lattice spacing $d_{\parallel}$ and unstrained lattice spacing d_i ($i=A$ or B):

$$d_{\perp i}=d_i-\frac{2C^i_{12}}{C^i_{11}}(d_{\parallel}-d_i) \qquad (1)$$

The $d_{\parallel}$ of the SLs may be written as below:

$$d_{\parallel}=\frac{G_AL_Ad_A+G_BL_Bd_B}{G_AL_A+G_BL_B} \qquad (2)$$

where G_i ($i=A$ or B) is the value represented as:

$$G_i=C^i_{11}+C^i_{12}-\frac{2(C^i_{12})^2}{C^i_{11}} \quad (i=A,\ B) \qquad (3)$$

For the ZnS $C^A_{11}=10.5\times10^{11}$ dyn/cm^2 and $C^A_{12}=6.53\times10^{11}$ dyn/cm^2, on the other hand, $C^B_{11}=8.50\times10^{11}$ dyn/cm^2 and $C^B_{12}=5.02\times10^{11}$ dyn/cm^2 for the ZnSe. So the ratio of the values G_A/G_B becomes 1.17. L_A and L_B are layer thickness represented by $N_Ad_{\perp A}$ and $N_Bd_{\perp B}$, respectively. ZnSe(ZnS) lattice constant in the direction perpendicular to the interface is elongated(shortened), while the one parallel to the interface is shortened(elongated).

Diffraction intensities can be calculated using the equation below:

$$I=\left| F_A \frac{1-\exp(i4\pi L_A \sin\theta/\lambda)}{1-\exp(i4\pi d_{\perp A} \sin\theta/\lambda)} + F_B \exp(i4\pi L_A \sin\theta/\lambda)\frac{1-\exp(i4\pi L_B \sin\theta/\lambda)}{1-\exp(i4\pi d_{\perp B} \sin\theta/\lambda)} \right|^2 \quad (4)$$

The SLs period can be determined accurately from the diffraction peak positions, and thickness of each layers and diffusion can be estimated so that the diffraction intensities fit to the experimental values. In our calculation we assumed that thickness of the each layer and period are integral multiples of the each layer and the period are integral multiples of the perpendicular lattice spacings. Real superlattice is not always represented by the integral multiple, and spacing of the peak positions sometimes deviates from the calculated values.

The intensity ratio of each peak of the SLs in Fig. 5 was compared with the area ratio of the peaks measured. As the results above mentioned, the calculated X-ray diffraction patterns agree with the measured ones.

Each scattering factor can be represented using scattering factors of Zn, S and Se layers. To calculate relative peak intensities we used the scattering factors calculated from the following equations:

$$F_A=f_{Zn}+f_S \exp(i2\pi d_{\perp A} \sin\theta/\lambda)$$
$$F_B=f_{Zn}+f_{Se} \exp(i2\pi d_{\perp B} \sin\theta/\lambda) \quad (5)$$

Real lattice spacing may be somewhat differ from the value calculated above owing to the strain from the substrates or other influences. Uniform deviation of the theoretical peak positions from the experimental values also occurs by the misestimation of the thickness or perpendicular lattice spacing of each layer. We used $d_{\parallel}$ as a fitting parameter introducing Δ in the Eq. (2) using the equation below:

$$d_{\parallel}=(1+\Delta)\frac{1.17L_A d_A+L_B d_B}{1.17L_A+L_B} \quad (6)$$

Strain from the substrate deviates the lattice spacing parallel to the layer, which somewhat deviates the superlattice period D and also diffraction angles according to $2D\sin\theta=n\lambda$. In the calculation of these samples we used (a) $\Delta=0.001$, (b) -0.001, (c) 0, (d) -0.001 and (e) -0.003 in Fig. 5 which give agreement between the experimental and the theoretical peak positions. The negative value of the Δ means that the superlattice layers have compressive strain from the GaAs(100) substrate. From the X-ray diffraction pattern it is calculated that the ratios of ZnS and ZnSe strain parallel to the interfaces are decreased with increasing the ZnS thickness for ZnSe one.

When interdiffusion of the constituents is taken into account, the lattice constants and scattering factors vary with the position according to the composition variation. Diffusion from a interface is written as $(1/2)\mathrm{erfc}(z-z_0)/\sqrt{Dt}$ (D: diffusion constant) using the error function complement [11]. In the discussion of the diffusion is independent of the depth (growth time), and defined the $\sqrt{Dt}$ as diffusion length. Interdiffusion length of S and Se is estimated to be less than 2 Å.

Fig. 6(b) and (c) are the calculated diffraction patterns using the strain equation to determine the thickness L_A, L_B of ZnS and ZnSe layers, respectively. Fig. 6(b) is the pattern calculated without taking into account Se-diffusion between ZnS and ZnSe layers, and Fig. 6(c) is the one calculated taking Se-diffusion into account. The insert of Fig. 6(c) indicates that Se is diffused into ZnS and ZnSe layer. These facts indicate that the intensity and the peak position of X-ray diffarction pattern are able to change due to the quantity of Se-diffusion. The interdiffusion length of the superlattice is estimated to be 2 Å. However, the calculated diffusion length may not give real diffusion length directly.

Although the intensities of the satellite peaks in Fig. 6(c) are different from the measured results, the positions of the peaks are approximately coincident with Fig. 6(a) and (b). Therefore, it is confirmed that the SLs of $(ZnSe)_2$-$(ZnS)_{24}$ monolayers are successfully grown on the GaAs(100) substrates.

Although the total number of the layer are almost the same, Fig. 7 shows X-ray diffraction patterns due to the difference of one monolayer in comparision with Fig. 7(b). Fig. 7 shows that if the number of each layers are different, the intensity and the

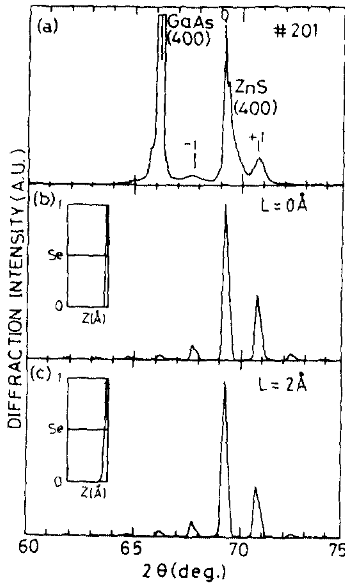

Fig. 6. X-ray diffraction pattern of ZnS-ZnSe SLs (a) measured, (b) calculated without taking Se-diffusion into account, and (c) calculated taking Se-one into account. The inserts show that Se is diffused into between ZnS and ZnSe interface.

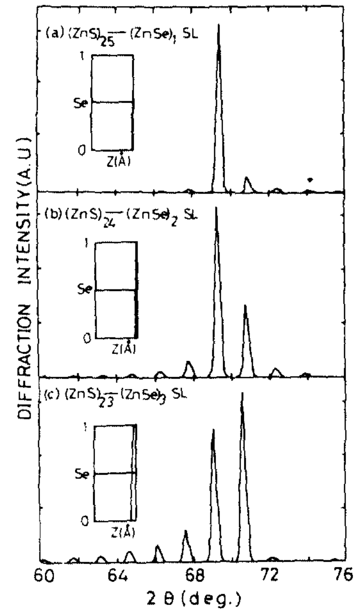

Fig. 7. X-ray diffraction pattern due to the difference of one monolayer. The inserts show that Se is diffused into between ZnS and ZnSe interface.

peak position of X-ray diffraction pattern of SLs change. The diffraction peak intensities vary very sensitively with the superlattice structure, and the calculated pattern of Fig. 7(b) is similar with the experimental pattern in the Fig. 6(a). However, the peak positions somewhat differ from the experimental ones. The peak positions are fitted by varying the Δ from zero as mentioned above. Thus X-ray diffraction gives very useful information determining the thickness of each layer and strain in the strained layer SLs.

Fig. 8 shows a model of the fluctuation or imperfection of the ZnS-ZnSe interface and resultant lattice spacing distribution. If there are atomic steps shown in the figure, the lattice spacing at the interface deviates and the diffraction intensities becomes similar to the interdiffusion. Thus real diffusion is considered to be smaller than the value calculated. In any any case, it is concluded that the interdiffusion of these ZnS-ZnSe SLs prepared by hot wall epitaxy is very small and the diffusion length is less than 2 Å.

3.2. Photoluminescence (PL)

Fig. 9 shows the PL spectra of ZnS-ZnSe SLs measured at 77 K. As seen from the figure, each spectrum almost consists of a dominant sharp line in the high energy region and of broad spectra in the lower energy region. The former is considered to be associatedwith band gaps of SLs. The latter is associated with deep level defects. The peak photonenergy increases with ZnS thickness owing to the quantum effect where the ZnS layers form barriers for both electrons and holes and with decreasing the ZnSe thickness at the same time. The intensity of the broad spectra is decreased more than one of the samples grown without the ZnS buffer layer. These facts indicate that ZnS-ZnSe SLs of the good quality are grown on the buffer ZnS layer, and deep level defects are decreased. Broad spectra become weak as the thickness of the ZnSe well layer is decreased and as one of the ZnS is increased.

This fact indicates that the carrier confinement should be enhanced and the compressive strain in the ZnSe layer is increased, which will suppress the introduction of defects. Fig. 10 shows the PL

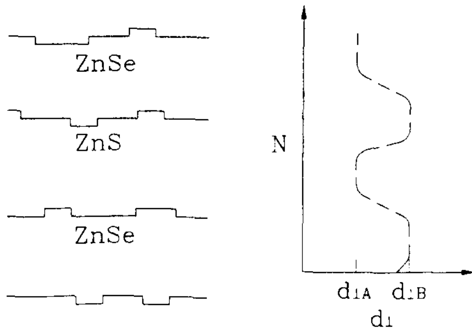

Fig. 8. A model of the fluctuation of the interface, which gives similar influence on the X-ray diffraction pattern of the SLs with the interdiffusion of the constituents.

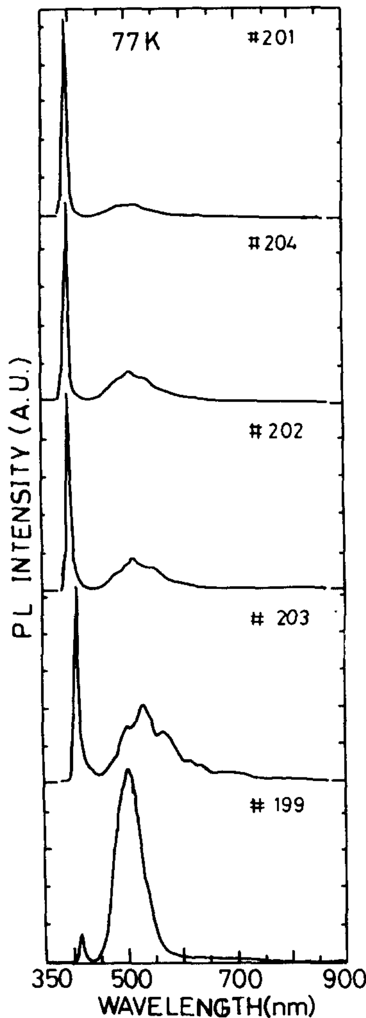

Fig. 9. PL of ZnS-ZnSe SLs measured at 77 K.

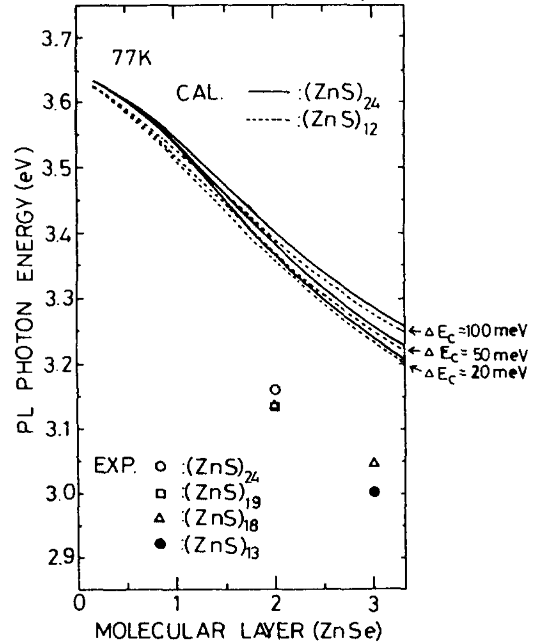

Fig. 10. PL photon energy compared with the energy band gap of ZnS-ZnSe SLs calculated using Kronig-Penney model at 77 K.

photon energy for the various kinds of SLs at 77 K. The experimental results are compared with the energy gap between $n=1$ electron and $n=1$ hole level of the SLs of the theoretical calculations using the Kronig-Penney model. The energy gap of SLs largely depends on the band offsets of the conduction and the valence band. Band offset ΔE_c in the calculation is assumed to be 100, 50, 20 meV, and for each energy of the conduction band offset the energy gap of ZnS-ZnSe SLs is shown in Fig. 10. The PL photon energy is not in good agrement with the calculated peak energy. Disagreement will be due to the strain effect on the ZnSe energy gap which decreases with the compressive strain and also on the band offset ΔE_c, which also decreases with the compressive strain. Fig. 10 shows that the binding energy of SLs depends on the thickness of ZnS layer. As the results of the calculation, ZnS-ZnSe SLs are considered to be type I, where both electrons and holes are confined in the smaller energy gap material, ZnSe.

4. Conclusions

ZnS-ZnSe strained-layer SLs were grown on GaAs(100) by HWE. The X-ray diffraction pattern showed satellite peaks indicating SLs structures. A sharp line emission originating from the recombination of carriers between the quantized levels in the ZnSe well layer was observed. These experimental results are compared with a Kronig-Penney model calculated taking into account the strain effect. These facts show that ZnS-ZnSe SLs are type I SLs.

Acknowledgements

One of the authors, Y. D. Choi, wishes to acknowledge KOSEF for financial support to perform this work.

References

1. H. Fujiyasu, H. Takahashi, H. Shimizu, A. Sasaki and H. Kuwabara, *Proceedings of the 17th International Conference on the Physics of Semiconductors* (Springer-Verlag, New-York) p. 539.
2. A. Shen, H. Wang, Z. Wang, S. Lu, *Appl. Phys. Lett.* **60**(21), 2640 (1992).
3. Y. Kawakami, T. Taguchi and A. Hiraki, *Appl. Surf. Sci.* **33/34**, 1059 (1988).
4. J. I. Pankove, *Electroluminescence* (Springer-Verlag, New York, 1977) p. 133.
5. H. Kuwabara, H. Fujiyasu, H. Shimizu, A. Sasaki and S. Yamada, *J. Cryst. Growth* **72**, 299 (1985).
6. G. C. Osbourn, *J. Appl. Phys.* **53**(3), 1586 (1982).
7. A. Taike, N. Teraguchi, M. Konagai and K. Takahashi, *Jpn. J. Appl. Phys.* **26**(6), L989 (1987).
8. A. Hobbs, O. Ueda, Y. Nishijima, H. Ebe, K. Shinohara and I. Umebu, *J. Cryst. Growth* **126**, 605 (1993).
9. H. Fujiyasu, A. Ishida, H. Kuwabara, S. Shimomura, S. Takaoka and K. Murase, *Surf. Sci.* **142**, 579 (1984).
10. H. Fujiyasu, T. Sasaya, M. Katayama, K. Ishino, A. Ishida and H. Kuwabara, *Appl. Surf. Sci.* **33/34**, 854 (1988).
11. A. Ishida, M. Aoki and H. Fujiyasu, *J. Appl. Phys.* **58**(2), 797 (1985).